

2D Materials



PAPER

Van der Waals interfaces in epitaxial vertical metal/2D/3D semiconductor heterojunctions of monolayer MoS₂ and GaN

RECEIVED
30 April 2018

REVISED
15 June 2018

ACCEPTED FOR PUBLICATION
6 July 2018

PUBLISHED
2 August 2018

Dmitry Ruzmetov^{1,7} , Mahesh R Neupane¹, Andrew Herzing², Terrance P O'Regan¹, Alex Mazzoni¹, Matthew L Chin¹, Robert A Burke^{1,3} , Frank J Crowne¹, A Glen Birdwell¹, DeCarlos E Taylor⁴, Andrei Kolmakov⁵, Kehao Zhang⁶, Joshua A Robinson⁶, Albert V Davydov² and Tony G Ivanov¹

¹ Sensors and Electron Devices Directorate, US Army Research Laboratory, Adelphi, MD 20783, United States of America

² Material Measurement Laboratory, National Institute of Standards and Technology, Gaithersburg, MD 20899, United States of America

³ General Technical Services, LLC, Wall Township, NJ 07727, United States of America

⁴ Weapons and Materials Research Directorate, US Army Research Laboratory, Aberdeen Proving Ground, MD 21005, United States of America

⁵ Center for Nanoscale Science and Technology, National Institute of Standards and Technology, Gaithersburg, MD 20899, United States of America

⁶ Department of Materials Science and Engineering and Center for Two-Dimensional and Layered Materials, The Pennsylvania State University, University Park, PA 16802, United States of America

⁷ Author to whom any correspondence should be addressed.

E-mail: dmitry.a.ruzmetov.civ@mail.mil

Keywords: molybdenum disulfide, gallium nitride, 2D/3D heterojunctions, TEM, Schottky barrier, contacts to 2D, *p*-GaN

Supplementary material for this article is available [online](#)

Abstract

A promising approach for high speed and high power electronics is to integrate two-dimensional (2D) materials with conventional electronic components such as bulk (3D) semiconductors and metals. In this study we explore a basic integration step of inserting a single monolayer MoS₂ (1L-MoS₂) inside a Au/*p*-GaN junction and elucidate how it impacts the structural and electrical properties of the junction. Epitaxial 1L-MoS₂ in the form of 1–2 μm triangle domains are grown by powder vaporization on a *p*-doped GaN substrate, and the Au capping layer is deposited by evaporation. Transmission electron microscopy (TEM) of the van der Waals interface indicates that 1L-MoS₂ remained distinct and intact between the Au and GaN and that the Au is epitaxial to GaN only when the 1L-MoS₂ is present. Quantitative TEM analyses of the van der Waals interfaces are performed and yielded the atomic plane spacings in the heterojunction. Electrical characterization of the all-epitaxial, vertical Au/1L-MoS₂/*p*-GaN heterojunctions enables the derivations of Schottky barrier heights (SBH) and drawing of the band alignment diagram. Notably, 1L-MoS₂ appears to be electronically semi-transparent, and thus can be considered as a modifier to the Au contact rather than an independent semiconductor component forming a *pn*-junction. The *I*-*V* analysis and our first principles calculation indicated Fermi level pinning and substantial band bending in GaN at the interface. Lastly, we illustrate how the depletion regions are formed in a bipolar junction with an ultrathin monolayer component using the calculated distribution of the charge density across the Au/1L-MoS₂/GaN junction.

1. Introduction

Two-dimensional (2D) semiconductors possess distinctive properties that attract considerable attention to this class of materials. Recently, they are playing a key role in the quest for new concept semiconductor electronic devices with advanced performance [1, 2]. With the electronics research happening mostly on the nanoscale domain, the

atomically-sharp interfaces and ultrathin dimensions of 2D semiconductors make them interesting candidates for novel nano-electronic components. Whether 2D semiconductors will be of utility in future electronics depends, in part, on how well they can be integrated with traditional electronic components such as conventional (3D) semiconductors and metals. A detailed examination of the nanostructure and electrical conductance of a 2D semiconductor

integrated in an epitaxial Au/2D/3D heterojunction is the subject of this paper.

Vertical devices based on 2D semiconductor heterostructures are of interest since they promise high speed and large power performance due to short current paths and large current cross-sections [3]. The integration of novel 2D semiconductors with established conventional materials in 2D/3D heterostructures has the potential to take advantage of both the unique properties of atomically sharp 2D crystals and the time-tested, mainstream 3D materials [4]. MoS₂ and GaN are suitable candidates for 2D/3D heterostructures. MoS₂ is one of the most studied 2D semiconductors since it is chemically stable and has desirable electronic and optical properties including an energy bandgap of 1.3–2.2 eV depending on the layer count [5, 6]. Suitable bandgaps and small mismatch in electron affinities of MoS₂ and GaN make possible the envisioning of their function in a vertical heterojunction bipolar transistor (HBT). In this case, an ultrathin 2D base would provide for short minority carrier diffusion times and thus fast performance [7, 8]. GaN is an important semiconductor for high speed and power devices and is currently used in wireless communications, radars, guided missiles, and electronic warfare systems [9]. Matching in-plane lattice constants and similar thermal expansion coefficients of MoS₂ and GaN promise low-defect epitaxial alignment between the two materials that is preserved upon the cooling of the sample from the growth to room temperature [3, 10]. The epitaxial nature of the growth of MoS₂ on GaN is important for the study of the vertical transport since the registry of the lattices of the two materials will provide an ordered, intimate, and reproducible interface desired for the low-scattering vertical charge transport.

There has been interest in the scientific community in MoS₂/GaN heterostructures as a model 2D/3D platform with a potential to electronics technology. Lee *et al* have demonstrated that a multilayer stack of *p*-MoS₂ grown by chemical vapor deposition (CVD) and transferred onto a *n*-GaN substrate works as a bipolar semiconductor diode with high degree of rectification [11]. Concurrently, epitaxial 1L-MoS₂ domains on *n*-doped GaN were grown by powder vaporization and electrical properties of such as-grown vertical 2D/3D heterojunctions were tested with conductive atomic force microscopy (CAFM) [3]. The close lattice match of GaN and some 2D transition metal dichalcogenides inspired using MoS₂ as a near-lattice-matched substrate for nitride growth [12]. Growing GaN on top of 2D is very relevant for the development of a vertical 3D/2D/3D heterostructure system, such as an HBT, where the emitter layer of GaN would be needed to be grown on the 2D. Along this direction, Tangi *et al* performed successful growth of GaN on top of 1L-MoS₂ when GaN was grown by molecular beam epitaxy (MBE) and 1L-MoS₂ was CVD-grown on sapphire [13]. Soon thereafter, MoS₂/

GaN Esaki tunnel diodes capable of large current density were fabricated with transferred multilayer *p*⁺ MoS₂ on *n*⁺ GaN grown by MBE [14]. In our recent work, the nanostructure of the heterojunction of epitaxial monolayer and bilayer MoS₂ on *n*-GaN was analyzed with TEM and good monolayer quality and close in-plane lattice match of MoS₂ and GaN were established [10]. Electrical characterization with CAFM of epitaxial 1L-MoS₂ grown directly on both *n*-doped and *p*-doped GaN and the comparison of the *I*–*V*s with bare GaN response for each type of doping were made. A switch of the rectification polarity depending on the GaN substrate doping was found. The consideration as a whole of the electrical behavior of several different tip-semiconductor combinations indicated that the charge transport across the CAFM-tip/1L-MoS₂/GaN interface was dominated by the character of the tip/GaN interface implying the 2D monolayer was electronically semi-transparent [10]. Last year, Henck *et al* investigated the electronic band structure of 1L-MoS₂/*p*-GaN heterostructure using angle resolved photoemission spectroscopy and high resolution XPS [15]. The 0.32 eV shift of the valence band in GaN towards the Fermi level was observed after the addition of the 1L-MoS₂ to the surface indicating the reduction of band bending (BB) in the 2D/3D heterostructure. We find a similar trend in our work as detailed below in the Results section. Recently, successful CVD growth of epitaxial 1L-MoS₂ on GaN was reported by other groups and interesting electron–phonon interaction effects were seen in their photoluminescence data [16].

The objective of this study is to explore how 2D semiconductors can be integrated with conventional components of RF electronic devices such as III–V semiconductors and metals. To this end, a 2D semiconductor is chosen in the form of single molecular layer thickness as the most basic case and in order to emphasize the novel effects that might arise due to the unique properties of 2D materials, such as ultrathin dimensions. We fabricate epitaxial Au/2D/3D and Au/3D semiconductor heterostructures in a similar process and analyze their properties. The first question that we explore is whether the 2D monolayer remains a distinct unperturbed component inside the heterostructure rather than alloys with the neighbor material layers or is disrupted by the physical and chemical interactions during the fabrication process. This issue is especially critical for a device of a vertical charge transport geometry. We address this question with cross-sectional TEM imaging of Au/1L-MoS₂/GaN and Au/GaN heterojunctions and obtain quantitative nano-structural information on the heterojunctions supported with first principles density functional theory (DFT) calculations. Our next test investigates the effect of the 2D monolayer on the electrical properties of the host Au/3D heterojunction. Current–voltage characteristics are measured with nanoprobe inside an SEM and a comparison of the electrical properties of the heterojunctions is made. Interestingly, the 2D monolayer

appears as a distinct layer in TEM images but behaves as an electronically semitransparent component inside Au/3D heterojunctions. The analysis of the I - V data was employed to draw band alignment diagrams of the heterojunctions. Finally, our first principles calculations, which are validated with the agreement with the TEM data, provide further insight into the physics of these heterojunctions. The calculations of the atom-projected density of states of Au/1L-MoS₂/GaN elucidate how the energy band of the interface states is formed inside the band gaps of MoS₂ and GaN. These calculated gap states support the presence of Fermi level pinning effect deduced from the electrical data. Furthermore, we address the notorious question on how the charge depletion regions in a bipolar 2D/3D junction can form when its 2D component is thinner than a typical depletion width in a conventional bipolar junction under zero bias. To do so we calculate the nanoscale charge density distribution in the Au/1L-MoS₂/GaN heterojunction and show that the depletion region extends beyond the 2D layer into the van der Waals (vdW) gaps and that the charge exchange mainly occurs across the MoS₂/Au interface while the GaN layer is effectively screened by the larger vdW gap. The results of this study improve the understanding of the interaction of 2D crystals with the components of traditional electronic devices, which is important for developing successful vertical 2D/3D heterostructure devices.

2. Methods

2D semiconductor growth. The domains of MoS₂ were grown on GaN substrates by a powder vaporization method which has been described previously [3]. Briefly, molybdenum trioxide (MoO₃) is placed in the center of a single zone furnace along with the GaN substrate, and sulfur powder is placed ~12 inches upstream of the MoO₃ crucible. The growth occurs in ultra-pure argon at 800 °C and 710 Torr for 15 min, with the sulfur heated separately by a heat tape at 130 °C. The GaN substrates were purchased from NTT-AT⁸ and consisted of a GaN film which was grown epitaxially by MOCVD on c -plane sapphire substrates. The GaN film is of 1.2 μm thickness and is p -doped with Mg dopants of 10¹⁹ cm⁻³ concentration. The resultant free-hole carrier density of p -GaN is $p \approx 10^{17}$ cm⁻³ as confirmed by NTT-AT.

Gold nanocontacts on MoS₂/GaN samples were fabricated by electron beam lithography (EBL) and physical vapor deposition (PVD). The arrays of circular nanodots of 600 and 400 nm diameter were patterned

in PMMA resist using a 100 kV beam with a dosage of ~850–1000 μC cm⁻² using a Vistec EBLPG5000 + ES EBL system. The dosed sample was then developed using a 1:2.5 ratio of methyl isobutyl ketone (MIBK) to IPA followed by an IPA rinse. No descum or any other plasma clean was used in order to prevent ion damage to the 2D monolayers. The deposition of a 60 nm Au layer was achieved in an e-beam evaporator (CHA Industries) at room temperature with a chamber pressure of 1 μTorr and a deposition rate of 2 Å s⁻¹. Lift-off was performed in an acetone bath for 4 h at room temperature.

TEM sample preparation was done using a FEI Helios NanoLab 660 dual-beam focused ion beam (FIB) and scanning electron microscope (SEM) system equipped with focused electron and ion beam induced deposition (EBID and IBID) capabilities. The focused EBID (or IBID) allows deposition of Pt or C in the areas patterned by the SEM electron beam (or FIB) with the help of a precursor gas injection system. A region of interest was *in situ* capped with C and Pt protection layers using EBID and IBID. A lamella slice containing a Au/MoS₂/GaN interface was ion milled with the FIB and extracted using an Oxford Omniprobe 300 manipulator and Pt welds by EBID. The lamella was EBID-welded to a TEM copper grid and consequently thinned by FIB to electron transparency.

Scanning transmission electron microscopy (TEM) was carried out using a spherical-aberration corrected FEI Titan 80–300 operating with a primary beam energy of 300 keV. High-angle annular dark-field (HAADF) images were collected using a detector inner collection angle of 70 mrad. The convergence angle of 13 mrad was achieved with a 40 μm probe forming aperture. Additionally, x-ray energy dispersive spectroscopy (XEDS) was carried out using a probe current of 0.3 nA and a side-entry silicon drift detector. Structural characterization was performed using electron nanobeam diffraction using a primary beam energy of 300 keV in a spherical aberration-corrected scanning transmission electron microscope (STEM). The convergence angle of approximately 3 mrad was achieved with an aperture size of 10 μm. The probe was positioned on the area of interest using the scan coils of the STEM and the resulting convergent-beam electron diffraction (CBED) pattern was collected using a CCD camera. The scales in the TEM line profile graphs were calibrated to the c lattice constant of GaN assuming its bulk value $c = 5.185$ Å based on our independent measurements and the literature [17].

Electrical measurements were performed inside a field emission SEM from Zeiss where the Au nanocontacts were accessed with Kleindiek Nanotechnik piezo-actuated nano-manipulators. Circular Au nanocontacts and MoS₂ monolayer domains were appraised with SEM. The selected nanocontacts were contacted with W nanoprobe of tip radius 150 nm and current-voltage characteristics were measured with a Keithley 238 programmable source-measure unit. Generally no

⁸Disclaimer: certain commercial equipment, instruments, or materials are identified in this document. Such identification does not imply recommendation or endorsement by the National Institute of Standards and Technology, nor does it imply that the products identified are necessarily the best available for the purpose.

noticeable damage was observed on the Au nanocontacts after W nanoprobe contact. The bottom contact to the MoS₂/p-GaN heterojunctions was enabled with large Ti/Au top contacts to p-GaN as warranted previously [3, 10].

Kelvin probe measurement was performed at room temperature in air on a kelvin probe system by KP Technology Ltd. The copper tip radius is approximately 1 mm. The measurement was performed in an enclosed dark chamber with no background illumination. A gold contact on the sample served as a calibration material.

3. Results and discussion

MoS₂ domains were grown on p-GaN substrates (*c*-plane GaN, thickness $th = 1.2 \mu\text{m}$, free-hole density $p \approx 10^{17} \text{ cm}^{-3}$; host substrate, *c*-plane sapphire, $th = 0.5 \text{ mm}$) by powder vaporization as described in the experimental section and elsewhere [3]. Our x-ray photoelectron spectroscopy (XPS) studies indicate that the as-grown MoS₂ is an *n*-type semiconductor [18]. Thus the synthesized MoS₂/p-GaN heterojunctions represent a case of a 2D/3D *np*-structure. The as-grown MoS₂ domains on p-GaN substrates underwent thorough structural characterization with SEM, atomic force microscopy (AFM), XPS, photoluminescence, and Raman spectroscopy as described elsewhere [3, 10] and were proven to be of good quality MoS₂. The MoS₂ domains covered ~40% of the GaN surface. The MoS₂ consisted of single, isolated triangles, predominantly of monolayer thickness (1L-MoS₂), as well as merged areas, second layer, and higher order stacks. An SEM image of 1L-MoS₂ domains is shown in figure 1(a) and a panoramic SEM image demonstrating the highly oriented growth is shown in figure S1 of the supplementary data (SD) (stacks.iop.org/TDM/5/045016/mmedia). Isolated MoS₂ domains were in the shape of equilateral triangles with its side typically of 1–3 μm in length. The triangle sides are found to be parallel to the *m*-plane of the GaN substrate lattice in ~99% of the time as discussed in the SD. The growth of MoS₂ aligned with respect to the underlying GaN lattice is evidence of epitaxy.

In order to form metal/2D/3D and metal/3D junctions, arrays of Au nanodots (600 and 400 nm diameter, 60 nm thickness, 2 μm period) were fabricated on the MoS₂/GaN/Sapp structures (figure 1). Au nanodots were only evaluated if they were either entirely on a MoS₂ triangle or entirely on bare GaN substrate to represent Au/1L-MoS₂/GaN or Au/GaN junctions, respectively. The fine specks around the Au nanodots that are visible in SEM (figure 1(b)) were determined by TEM to be Au nano-particles scattered on top of the MoS₂, GaN, and nanodots from the final dot fabrication step and did not affect the conclusions of this study.

Cross-sectional characterization of the 2D/3D heterostructures was performed with scanning TEM. The sample area selected for TEM is shown with the green rectangle on the SEM image in figure 1(b) and consists of three Au nanocontacts on a MoS₂ domain and bare p-GaN. The TEM image of the prepared cross-section is shown in figure 1(c). The central Au nanocontact in figure 1(c) lies on a MoS₂ domain while the two side nanocontacts lie on bare p-GaN substrate as seen in figure 1(b).

The TEM of the interface under the central Au dot (see figures 1(b) and (c)) that lies on a MoS₂ domain is shown in figure 2(a). The TEM image shows the atomic planes in Au nanocontact, 1L-MoS₂, and GaN substrate parallel to the interface. The TEM of the interface near the edge of the Au nanodot illustrates that GaN/MoS₂ structure remains unperturbed when the Au nanodot is added (figure 2(b)). For comparison, the Au/semiconductor interface of the Au nanodot on bare GaN is shown in figure 2(c). The TEM analysis proves the monolayer nature of the MoS₂ domain extending throughout the whole undersurface of the central Au nanodot.

We used high magnification TEM images (e.g. figure 3(a)) to extract the lattice constants of the materials in the vertical structure. The in-plane lattice constants of GaN and 1L-MoS₂ were calculated from the TEM images using fast Fourier transform (FFT) of the averaged line intensities and were found to be $a = 3.175$ and 3.188 \AA respectively, which constitutes only a 0.4% lattice mismatch. The value of the measured in-plane atomic period $3.175/2 \text{ \AA}$ is within 0.4% of the literature value of the lattice constant of GaN ($a = 3.189 \text{ \AA}$) [17] and confirms the orientation of the cross-sectional plane in the GaN substrate which is *m*-plane ($1 \bar{1} 0 0$), as intended. The central Au nanodot in figure 1(b), which lies on 1L-MoS₂, is found to have distinct uninterrupted atomic planes throughout the Au dot. The only small grains observed inside the nanodot are found near the edges away from the substrate. The vertical period of the atomic planes in the central Au dot is measured to be 2.26 \AA which corresponds to the Au lattice $a_{\text{Au}} = 3.91 \text{ \AA}$ oriented with $[1 1 1]$ direction along the *c*-axis $[0 0 0 1]$ of GaN. The measured Au lattice parameter $a_{\text{Au}} = 3.91 \text{ \AA}$ is within 4% of the literature value of 4.065 \AA for bulk Au. The in-plane atomic period of the Au nanodot was calculated with FFT from the TEM images to be 2.91 \AA . This value corresponds to the viewing direction in the TEM images (GaN $[1 0 \bar{1} 0]$) to be along the Au $[\bar{1} \bar{1} 2]$ direction. These data indicate epitaxial alignment of the central Au nanodot to GaN. The epitaxy was confirmed with the convergent beam electron diffraction (CBED) measurements in TEM. The CBED images of the central Au nanodot on GaN/1L-MoS₂ showed alignment of the Au lattice to the GaN substrate, while the single crystal nanodot on bare GaN produced a misaligned diffraction pattern (figure S2). The peak

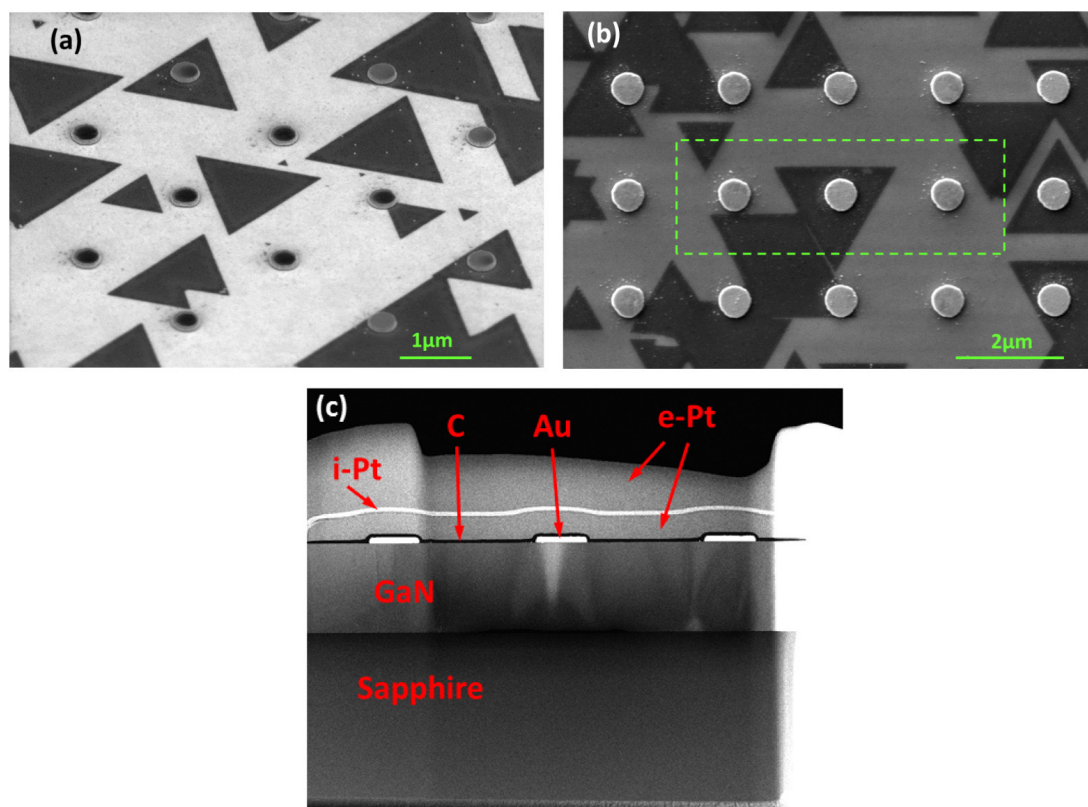


Figure 1. Top and side views of the Au/2D/3D and Au/3D junctions. (a) and (b) SEM images of triangular 1L-MoS₂ domains on a GaN substrate with circular Au nanocontacts. (b) The green rectangle shows the area that was selected for TEM characterization in this study. (c) Cross-sectional TEM image of the lamella slice extracted from the green rectangle area in (b). The gold pad lengths in (c) are 600 nm.

simulation and assignment for the GaN substrate and epitaxial Au nanodot were performed (see figure S2) using SingleCrystal[®] from CrystalMaker Software Ltd, which determined the following epitaxial alignment: Au[1 1 1] aligns with GaN[0 0 0 1]; Au[2 $\bar{2}$ 0] aligns with GaN[1 $\bar{2}$ 1 0] with a -8% lattice mismatch. Interestingly, the left (in figures 1(b) and (c)) non-epitaxial gold nanodot on bare GaN is found to be of multigrain nature with different grain orientations whereas the right nanodot on bare GaN is predominantly a single crystal but of misaligned orientation as shown in figure S2(c).

All three materials in figure 2(a), Au, 1L-MoS₂, and GaN, have atomically sharp interfaces that do not intermix. The ability to fabricate metal contacts to a single 2D semiconductor monolayer without disrupting its structural integrity is important for the development of functional electronic devices based on 2D crystals, especially for the case of devices with vertical charge transport. Yet, to our knowledge, there has been little direct evidence (such as high resolution TEM) before this work that such metal/2D interfaces were possible. Generally, various semiconductor processing steps, such as plasma treatments, high impinging energies of PVD-deposited metal atoms, diffusion, and chemical reactions are expected to pose risks to the integrity of the 2D monolayer. As an example, last year Kim *et al* provided rare cross-sectional TEM images of metal/1L-MoS₂ contacts and found that Pd

and Ti contacts to 1L-MoS₂ on a SiO₂ layer resulted in a distortion of the 1L-MoS₂ [19]. A disrupted metal/2D interface can be tolerated in lateral devices or stacks of several 2D layers but is unacceptable for vertical devices comprised of a single monolayer when direct shorts of the surrounding materials through the monolayer would negate the function of the 2D material. To avoid physical ion damage to the 2D layer, we eliminated the plasma clean steps in our nanodot fabrication process and chose a low impinging energy PVD process such as evaporation (*vis-à-vis* sputtering). In order to mitigate chemical interaction and inter-diffusion of the metal into the 2D layer, we chose Au as the contact material. Au is believed to create a less intimate contact to 2D MoS₂ than high adhesion materials (such as Ti and Cr) which are likely to disturb a single monolayer. In the computational study of Kang *et al*, vdW gaps between several metal contacts and MoS₂ were investigated [20]. The authors predicted Au contacts to have larger physical separation and lower level of hybridization with the 2D material as compared to some other common contact metals, such as Ti, Mo, and Pd. Au has been used by the 2D scientific community to deposit contacts to MoS₂ but there are scarce data published on the nanostructure of the Au/MoS₂ interface. In the study of Gong *et al* [21], ultrathin (2 nm) Au films were deposited by PVD onto MoS₂ and were reported to be of a discontinuous and granular nature, unlike what we see in our case.

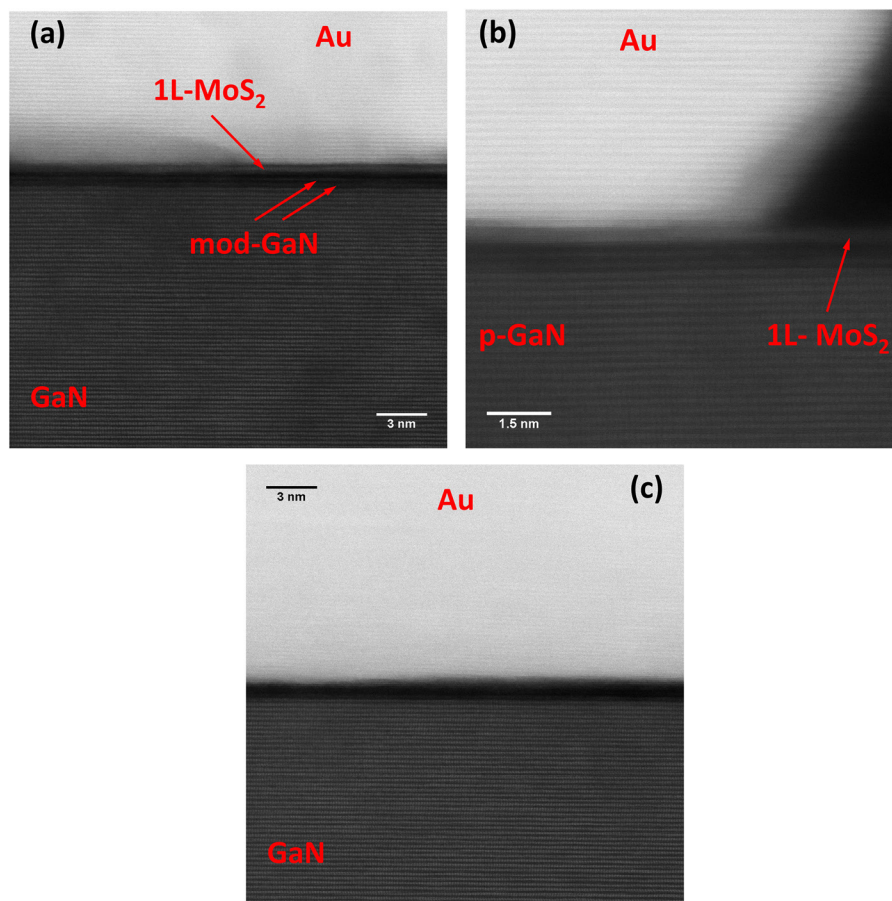


Figure 2. Cross-sectional TEM images of (a) and (b) the Au/1L-MoS₂/p-GaN hetero-junction and (c) the Au/p-GaN junction.

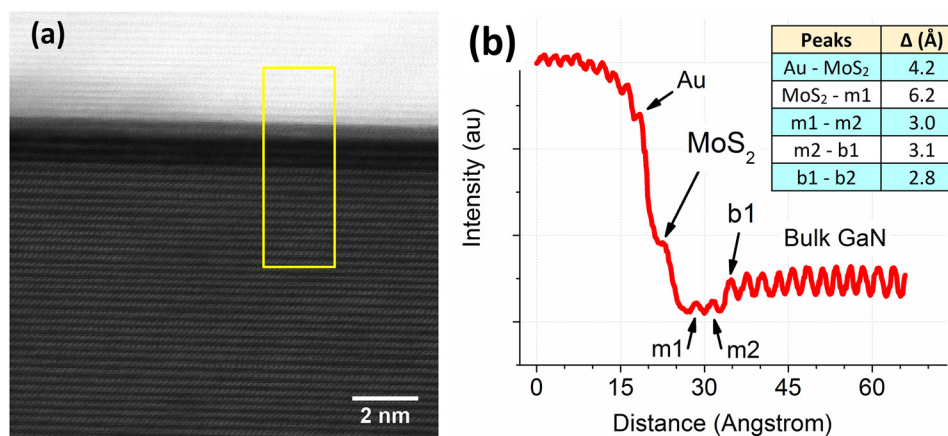


Figure 3. Cross-sectional TEM image analysis of the Au/1L-MoS₂/p-GaN interface. (a) A micrograph of the interface that includes the MoS₂ layer and two modified GaN layers. The yellow rectangle specifies the area used for the line profile in (b). (b) An averaged line profile of the TEM image intensity perpendicular to the interface and averaged along the interface within the yellow rectangle.

We speculate that the epitaxial growth of Au, dictated by the alignment of the MoS₂ and the whole hetero-junction to the GaN lattice, is essential for the continuity of the Au film and order at the Au/MoS₂ interface seen in our system.

The top two atomic layers of the GaN, which represent the height of one unit cell of the GaN lattice, appear to be modified in the areas beneath the MoS₂ monolayer. As was previously reported for *n*-doped

GaN [10], the modification in *p*-GaN is purely restricted to areas where MoS₂ is present and is not observed on the bare GaN. These two modified layers at the interface are labeled ‘mod-GaN’ in figure 2(a). In a separate TEM/EDS study the modified atomic layers are determined to be a GaN crystal diluted with sulfur and molybdenum. Details concerning these findings will be published in a future article by Burke *et al* [22]. The modified layer is ultra-thin and we do not expect S

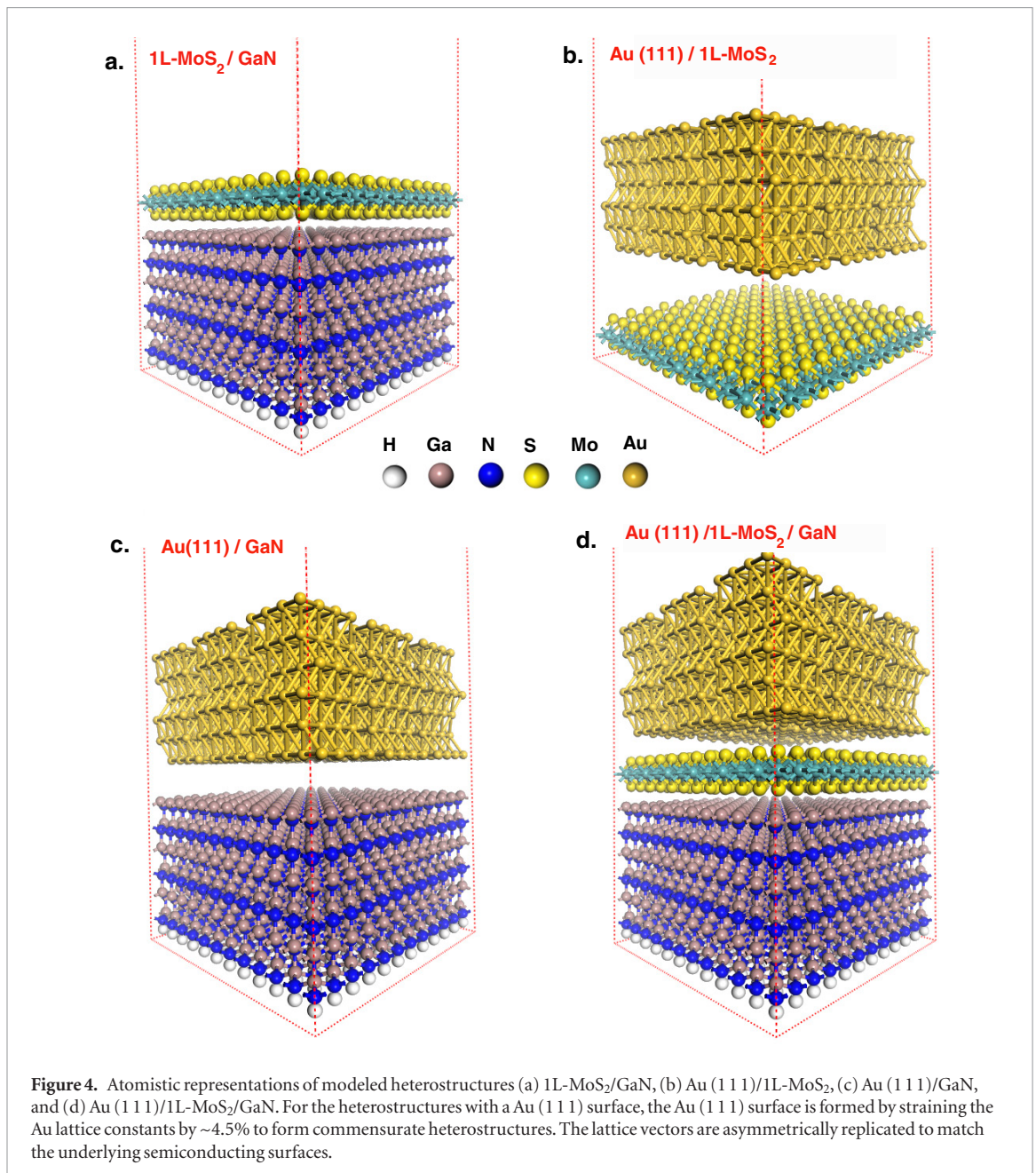
and Mo to be efficient dopants in GaN [23]. Therefore, the superficial layer in GaN is not expected to significantly affect the electrical properties of the GaN side of the heterojunction.

We performed quantitative TEM characterization of the Au/2D/3D interface in order to evaluate the vdW gap and other parameters of the heterojunction. Averaged TEM intensity line scans were extracted from the images, as shown in figure 3, where a yellow rectangle on the TEM image denotes the area examined. The line intensity profile was plotted perpendicular to the interface (i.e. along the long edge of the rectangle). The intensity at each point of the plotted line scan is an average along the line parallel to the interface within the rectangle. The first Au layer, MoS₂ monolayer, modified GaN layers (*m1*, *m2*), and first bulk GaN layer (*b1*) are denoted in the line profile of figure 3(b). Atomic plane spacings Δ were determined from the line profile and summarized in the inset table. The atomic spacings Δ were measured this way in over 20 locations at the interface of the epitaxial nanodot. For the distance between the MoS₂ and the 1st atomic Au layer above MoS₂ (*a1*), we get the value averaged over multiple locations $\Delta(a1 - \text{MoS}_2) = 4.5 \pm 0.4 \text{ \AA}$, where the uncertainty is the standard deviation for different measurements and represents the variation of the actual spacing and error of the measurement. The distance Δ is measured from the peak of the TEM intensity, i.e. between the centers of Mo and Au atom rows. Similarly, the MoS₂–GaN spacing is $\Delta(\text{MoS}_2 - m1) = 6.1 \pm 0.3 \text{ \AA}$. Assuming $\Delta(\text{Mo} - \text{S}) = 1.5 \text{ \AA}$ as the Mo–S bond distance and keeping in mind that our GaN is Ga-terminated, the MoS₂–GaN vdW gap can be estimated as $\delta(\text{S} - \text{Ga}) = \Delta(\text{MoS}_2 - m1) - \Delta(\text{Mo} - \text{S}) = 4.6 \pm 0.3 \text{ \AA}$. This δ value is larger than the one measured previously for the GaN/MoS₂ system without the Au capping layer, 3.1 \AA [10]. We speculate that the presence of the top Au layer above MoS₂ could be reducing the adhesion strength of the MoS₂ and GaN. A precise measurement of δ in the absence of the Au capping layer for the sample studied in this work could not be done because of the ion damage to the MoS₂ during the FIB sample preparation (see the surface area outside the nanodot in figure S5). The Au nanodot served, in part, as a protective mask during the TEM sample preparation. Next, the distance between the atomic layers in the modified GaN layers is measured to be $\Delta(m1 - m2) = 3.1 \pm 0.2 \text{ \AA}$ which is larger than the spacing between bulk GaN layers that varies within $\Delta(b2 - b3) = 2.6 \pm 0.2 \text{ \AA}$.

To gain further insight into the structural properties of the studied Au/2D/3D heterostructure system, we performed a systematic theoretical study of 2D/3D, Au/2D, Au/3D, and Au/2D/3D heterojunctions based on first-principles method using the projector augmented wave (PAW) method [24] as implemented in the Vienna *ab initio* simulation package (VASP) code [25]. The details of the calculations are described in the

SD, and the simulated heterostructures are shown in figure 4. First, the GaN/1L-MoS₂ heterostructure was considered in order to assess the vdW gap between 1L-MoS₂ and GaN in the absence of the Au contact. The atomistic model of 2D/3D (see figure 4(a)) was created using optimized bulk lattice parameters for wurtzite-GaN, $a = b = 3.22 \text{ \AA}$ and $c = 5.25 \text{ \AA}$, and bulk MoS₂, $a = b = 3.19 \text{ \AA}$ and $c = 12.33 \text{ \AA}$, which are consistent with earlier published experimental data [10, 26]. In order to create 2D/3D and metal/2D/3D heterostructures with desired in-plane periodicity and minimal surface induced features in the structural and electronic properties, we have used a slab-model of both the metal and 3D surfaces by checking their thickness convergence against their bulk properties, as described in our earlier study [10]. The detail concerning implemented methods and parameters used to design commensurate, strain-compensated Au/2D, Au/3D and Au/2D/3D heterostructures is presented in the SD. The vdW-spacing between the 2D and 3D layers was optimized, and an equilibrium vdW-gap of 3.1 \AA between the 1L-MoS₂ and GaN surface was calculated, which is consistent with our previous TEM observations [10]. Prior to designing a metal/2D/3D heterostructure, metal/2D and metal/3D heterostructures are individually optimized. The optimized vdW gaps for Au/1L-MoS₂ (see figure 4(b)) and Au/GaN (see figure 4(c)) heterostructures are 3.3 \AA and 3.25 \AA , respectively, indicating physisorbed nature of the metal/2D and metal/3D interfaces. We can compare the calculated Au/MoS₂ vdW gap $\delta_{theor}^{met/2D} = 3.3 \text{ \AA}$ with our TEM measurement result $\Delta(a1 - \text{MoS}_2) = 4.5 \pm 0.4 \text{ \AA}$. The vdW gap will be Δ minus the Mo–S bond length 1.5 \AA which yields $\delta_{TEM}^{met/2D} = 3.0 \pm 0.4 \text{ \AA}$ consistent with the calculated value. Using these optimized geometries and vdW gaps, we designed a Au/1L-MoS₂/GaN heterostructure, as shown in figure 4(d), and further optimized the vdW gap between 1L-MoS₂ and GaN layer in Au/1L-MoS₂/GaN heterostructure, by fixing the Au/1L-MoS₂ gap. The resultant equilibrium vdW gap for 1L-MoS₂/GaN interface in Au/1L-MoS₂/GaN is $\delta_{theor}^{2D/3D} = 4.0 \text{ \AA}$, a ~30% increment in vdW gap as compared to isolated 1L-MoS₂/GaN system reported earlier [10]. Quantitatively, the difference in observed (see above) and predicted $\delta^{2D/3D}$ with the Au contact is $0.6 \pm 0.3 \text{ \AA}$, a difference of ~13%. Though the increase caused by the Au contact of the vdW gap between 1L-MoS₂ and GaN layers observed in experiment is correctly captured in simulation, a quantitative agreement between observed and calculated vdW gaps demands for a comprehensive relaxation of Au/1L-MoS₂/GaN, which is outside the scope of this study.

It was noted in the TEM images that the wetting of the Au nanodot of the substrate changes depending on whether the dot is on MoS₂ or bare GaN, see figure S5. The contact angle of the Au nanodot on bare GaN was measured to be $\vartheta = 152^\circ$ and the contact angles on the left and right sides of the central nanodot on MoS₂/



GaN are $\vartheta = 112^\circ$ and 130° . Thus we observe an improved adhesion of Au to the GaN substrate when it is covered with 1L-MoS₂. To understand this enhanced binding characteristics of Au contact with and without MoS₂ on GaN during fabrication, we performed first principle calculations of Au on MoS₂ and Au on MoS₂/GaN heterostructures and compared their formation/adsorption energies, which is defined as the total energy difference between the heterostructure and the sum of its constituent layers. To rule out any method and simulation parameters dependent effect on the total energy calculation, we performed a static energy calculation by using similar first-principles related parameters, such as k-point grids, cutoff energies, and smearing parameters, and by maintaining equilibrium vdW gaps between the Au–MoS₂, MoS₂–GaN, and Au–GaN layers at 3.3, 3.1, and 3.25 Å, respectively. The calculated adsorption energy difference of -4.5 eV (-0.56 eV/surface atom) between

Au/1L-MoS₂/GaN and Au/GaN heterostructures indicates stronger binding of the Au, 1L-MoS₂, and GaN surfaces in Au/1L-MoS₂/GaN heterostructure as compared to Au and GaN surfaces in a Au/GaN heterostructure. This is expected, because the dangling Ga bonds on a GaN surface introduce a polarization force at the surface, which in turn contributes to the repulsion of Au layer. In contrast, adding MoS₂ layer in between GaN and Au surface passivates the dangling Ga bonds while suppressing polarizability of the surface, resulting in relatively stronger binding between the GaN and Au surfaces. A further study on the effect of metal and insertion layer types in order to improve adhesion of the Au contact to the GaN substrate may be of interest for metal contact engineering in 2D/3D heterostructures.

Figure 5(a) shows a SEM image of a Au/(1L-MoS₂)/*p*-GaN heterojunction contacted with a W nanoprobe. Au nanodots that lay entirely inside

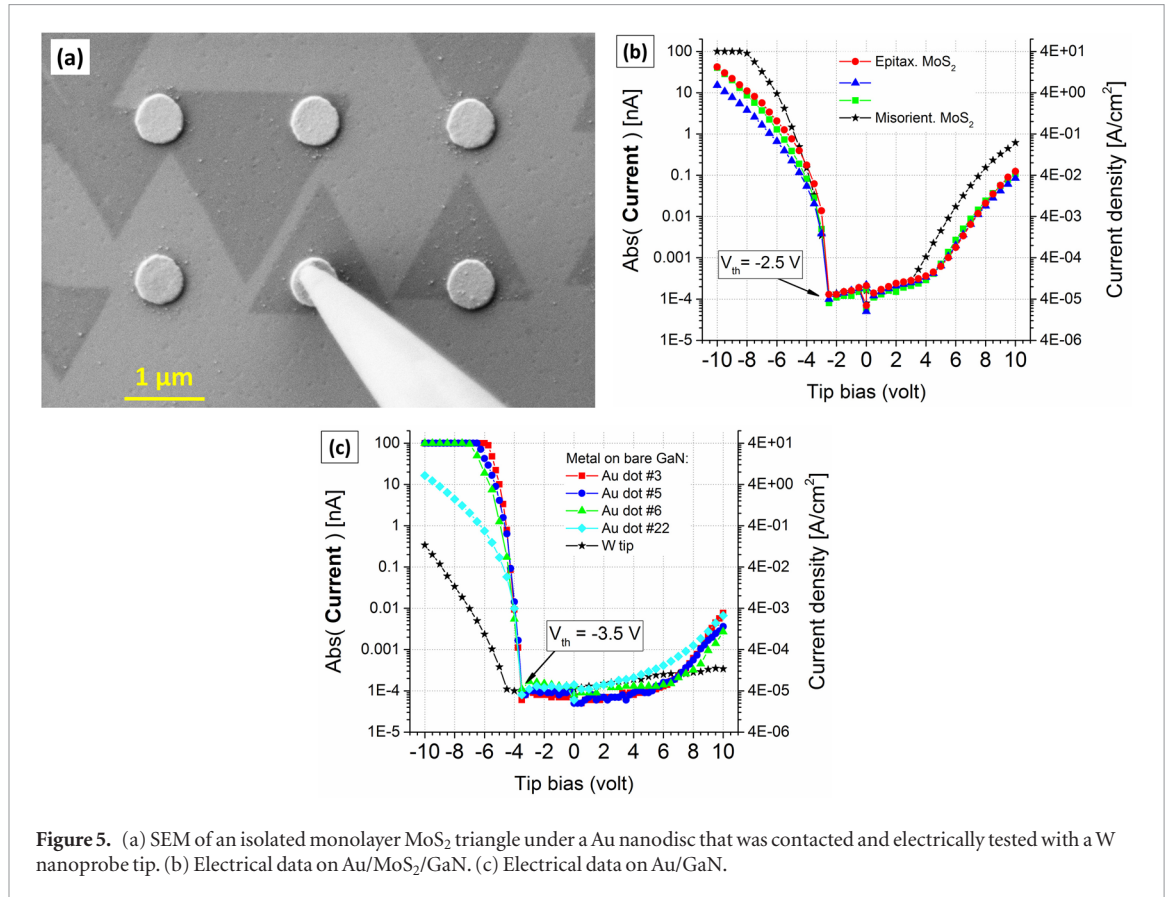


Figure 5. (a) SEM of an isolated monolayer MoS₂ triangle under a Au nanodisc that was contacted and electrically tested with a W nanoprobe tip. (b) Electrical data on Au/MoS₂/GaN. (c) Electrical data on Au/GaN.

a single isolated 1L-MoS₂ triangle were selected for the I - V measurements, and over a dozen of such Au/(1L-MoS₂)/ p -GaN heterojunctions were measured and analyzed. Current-voltage characteristics of several representative Au/(1L-MoS₂)/ p -GaN vertical heterojunctions are displayed in figure 5(b). The I - V measurements show rectification behavior. We attribute the electrical characteristics of the heterojunctions to be primarily determined by the nanodot/GaN junction which is perturbed by the insertion of a 1L-MoS₂. This physical picture was proposed in our earlier study after the analysis of the metal/1L-MoS₂/GaN electrical characteristics measured by CAFM on both p - and n -doped GaN and bare metal/GaN junctions [10]. This is in contrast to the picture for a thick MoS₂ layer where the MoS₂ acts as an independent semiconductor in the heterojunction forming two separate junctions on the Au and GaN interfaces.

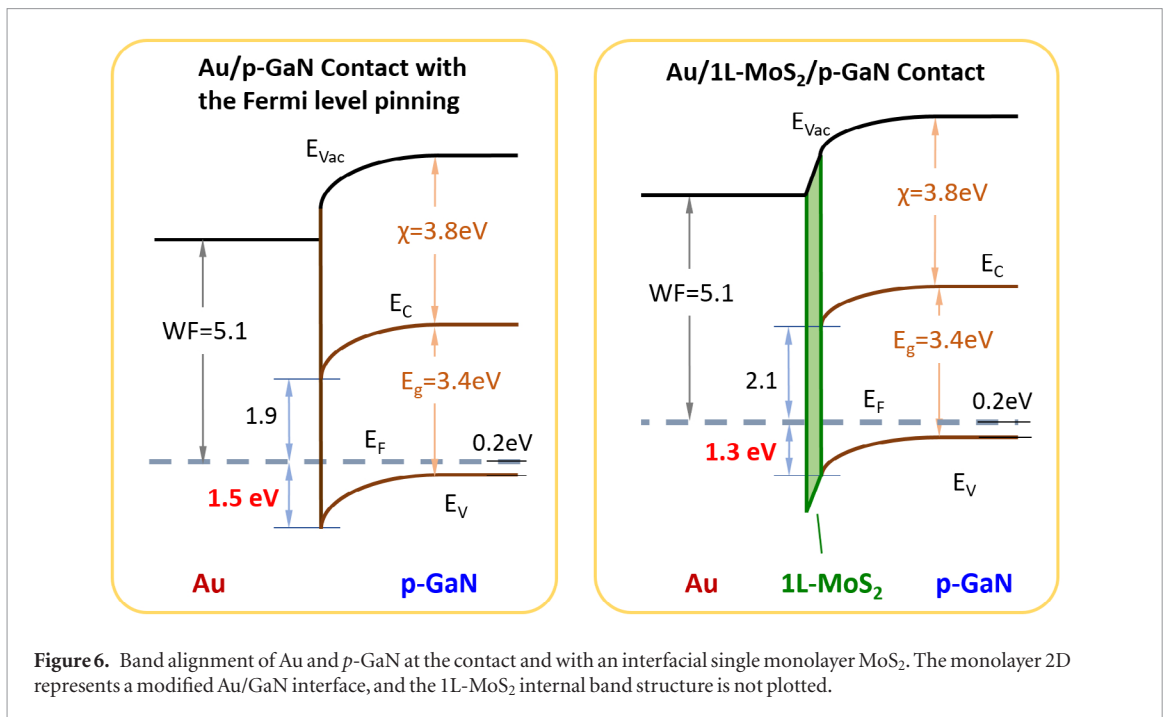
The electrical data involving permanent Au contacts on MoS₂/ p -GaN are considerably more reproducible and less noisy than our earlier CAFM data [3, 10], therefore the fine details of the I - V characteristics can be extracted and analyzed. The rectification polarity in figures 5(b) and (c) is consistent with a p -type Schottky barrier (SB). The forward bias on the Au/ p -GaN SB corresponds to the negative bias on the W nanoprobe (i.e. the Au nanodot). A striking feature in the I - V s is that all Au/(1L-MoS₂)/ p -GaN heterojunctions show the same distinct turn on (threshold) voltage at $V_{th} = -2.5$ V applied to the Au contact and the same slope near V_{th} . No devia-

tions from the $V_{th} = -2.5$ V turn on voltages on the forward Schottky bias were observed for over a dozen nanodots tested, including nanodots on isolated MoS₂ triangles and on merged triangle clusters that are believed to be of monolayer thickness as well. For comparison, the I - V s for the nanodots on bare GaN are plotted in figure 5(c). A similar distinct value of the turn on voltage is measured for Au/ p -GaN junctions with $V_{th} = -3.5$ V. Again, approximately ten dots (measurements) were tested and all of them displayed the -3.5 V turn-on voltage (V_{th}).

The high reproducibility of the V_{th} value and the I - V slope near V_{th} indicate that those parameters are determined mainly by the materials involved (Au/MoS₂/ p -GaN or Au/ p -GaN) and are not affected by the 2D domain sizes, quality of the probe/dot contacts, or various uncertainties of the measurements. The slope of the I - V curve near V_{th} was used to evaluate the effective SBs (Φ_B) assuming a thermionic emission model [27, 28],

$$I = A_{dot} A^* T^2 e^{-\frac{q\Phi_B}{kT}} e^{\frac{qV}{nkT}} \quad (1)$$

where $A_{dot} = 0.3 \mu\text{m}^2$ is the area of the Schottky contact ($\varnothing 600$ nm), $A^* = 120 \cdot (m^*/m_e) \text{ A cm}^{-2} \text{ K}^{-2} = 260 \text{ A cm}^{-2} \text{ K}^{-2}$ is the Richardson constant [27] of GaN based on an effective hole mass of $m_h^* = 2.2m_e$ [29, 30]. T is the absolute temperature, n is the ideality factor, $q = 1.6 \times 10^{-19}$ C, and k is the Boltzmann constant. Examples of the exponential curve fitting near the forward bias threshold are shown in figure S6. The extracted fitting parameters are $\Phi_B = 1.3$ eV and



$n = 4.5$ for Au/MoS₂/*p*-GaN and $\Phi_B = 1.5$ eV and $n = 4.5$ for Au/*p*-GaN. Therefore the analysis of the *I*-*V* characteristics within the model of thermionic emission over a Au/GaN SB yields that the insertion of a 1L-MoS₂ on the Au-GaN interface effectively reduces the SB by 0.2 eV.

The large value of the extracted ideality factor n indicates that there might be other physical mechanisms present behind the electron transport in addition to, or instead of, the thermionic emission. There are scarce electrical data in the literature for the metal/(1L-MoS₂)/GaN system. For thick (~ 10 nm) MoS₂ flakes contacted by metals, a significant contribution from tunneling across the metal/MoS₂ Schottky and tunnel barriers in addition to the thermionic emission has been demonstrated [31]. Even though the system with 1L-MoS₂ is different, a similar tunneling mechanism could be present in our case as well. Since the electrical behavior of the Au/(1L-MoS₂)/GaN heterojunctions is governed by the Au/GaN contact, we can compare our results with the literature data on Au/GaN and other metal/(3D semiconductor) junctions. A model based on equation (1) was successfully used to characterize Pt/*n*-GaN macroscopic Schottky diodes and a large number of nanoscale Schottky contacts created with a CAFM tip [28]. Further insight can be gained from a thorough study by Card and Rhoderick, where metal/semiconductor contacts were explored and insulating SiO₂ films of various thicknesses were introduced at the interface [32]. It was found that with the presence of an oxide layer, the general formula of equation (1) still held for the forward bias with increased parameters n and Φ_B . The increase in the oxide thickness resulted in a continuous increase in the ideality factor n and the oxide barrier height. The latter effectively increased the coefficient Φ_B in equa-

tion (1) with respect to the true metal/semiconductor SB. Additionally, the deviation of the *I*-*V*s from the exponential was progressively more pronounced in the same manner as in the *I*-*V*s in the figures 5(b) and (c) (i.e. the decrease of the slope at a larger forward bias on a semilog *I*-*V* plot). It is reasonable to conclude that the large values of the ideality factors extracted from our *I*-*V* plots and the deviation from the exponential behavior are the result of the presence of an insulating layer at the Au/GaN and 1L-MoS₂/GaN interfaces. For the case of *p*-doped semiconductors, the presence of an interfacial oxide layer between a metal contact and *p*-GaN was suggested as well using capacitance-voltage characteristics (*C*-*V*s) analysis [33]. To summarize, the absolute values of the effective SBs ($\Phi_B = 1.3, 1.5$ eV) extracted using equation (1) may be overestimates if a significant insulating layer is present at the interface with GaN. A more secure result of the analysis of the measured *I*-*V* data displayed in figure 5 is the 0.2 eV relative decrease of Φ_B upon the insertion of a 1L-MoS₂ on the Au/*p*-GaN interface. To illustrate these results, we plot a band diagram of the Au/*p*-GaN and Au/MoS₂/*p*-GaN heterojunctions in figure 6 based on the SB values available to us from the above *I*-*V* analysis.

The band diagram in figure 6 assumes literature values for the basic parameters of bulk Au and GaN and matches them with the measured SBs on the interface. The work function (WF) of the Au is assumed to be 5.1 eV [27], and the band gap of GaN is $E_g = 3.4$ eV [34]. The reported values for electron affinity of GaN vary between $\chi = 2.6$ to 4.1 eV [34–39] with the lower values of affinities generally measured for surfaces prepared in ultra-clean conditions. An $\chi = 3.8$ eV [36] is assumed in figure 6. The free-hole carrier density of *p*-GaN used in this study is $p \approx 10^{17}$ cm⁻³. The position

of the Fermi level (E_F) with respect to the top of the valence band (E_V) in bulk p -GaN can be estimated with the formula [17] $E_F - E_V = kT \cdot \ln N_V/p = 0.17$ eV, where $N_V = 8 \times 10^{19} \text{ cm}^{-3}$ is the effective density of states in the valence band of GaN calculated with an effective hole mass of $m_h^* = 2.2m_e$ [29, 30]. Within the Schottky–Mott approximation [27], the SB height for Au/ p -GaN is expected to be $E_g + \chi - \text{WF}_{\text{Au}} = 2.1$ eV which exceeds the measured value $\Phi_B \approx 1.5$ eV. We propose that there is Fermi level pinning at the Au/GaN interface that is reflected in figure 6 as a discontinuity in the vacuum level at the interface due to the presence of trapped charges on it. The insertion of a MoS₂ monolayer modifies the pinning and reduces the SB by 0.2 eV.

The SB heights extracted from our electrical measurements ($\Phi_B = 1.3, 1.5$ eV) are substantially lower than the Schottky–Mott approximation value (2.1 eV). This is in contrast to the Ni/ p -GaN system reported in the literature, where a large $\Phi_B \approx 2.8$ eV extracted from the electrical testing appears to be close and even above their Schottky–Mott values [33]. In order to validate our SB numbers, we made independent measurements of the band bending (BB) at the surface of our GaN substrates. We performed kelvin probe (KP) measurements with a macroscopic tip (\varnothing 2 mm) of the WF of a bare p -GaN wafer under atmospheric conditions relative to a Au contact. The measured WF at the surface of p -GaN is 6.20 ± 0.05 eV which is relative to the Au standard of 5.1 eV. The BB on the bare p -GaN surface can be calculated as the difference of the surface WF from the bulk value ($E_g + \chi - 0.17$ eV ≈ 7.0 eV): $\text{BB} = 7.0 - 6.2$ eV = 0.8 eV. The KP result for the BB in our p -GaN agrees with the literature values for the surface BB of bare p -GaN of 0.8 eV when measured with photoelectron spectroscopies [35, 39]. On the other hand, for the Au/GaN contact the electrically measured SB height yields BB of 1.3 eV, see figure 6. The larger BB of 1.3 eV extracted from our I - V analysis is likely due to the presence of the Au capping layer. The insertion of 1L-MoS₂ in between GaN and Au effectively increases the separation between the metal and 3D semiconductor and relaxes the BB in GaN towards its bare surface value. The reduced BB measured with KP is in accord with our I - V analysis results (i.e. the reduced SB heights) and can be explained with the presence of trap states on the interface resulting in the Fermi level pinning as illustrated in figure 6.

It is instructive to compare our electrical results with a recent study by Henck *et al*, involving characterization of the 1L-MoS₂/ p -GaN band structure via ARPES/XPS [15]. The BB in GaN was found to decrease from 1.9 eV to 1.6 eV after the transfer of a 1L-MoS₂ on p -GaN. Thus, the researchers found a 0.3 eV decrease of the BB in GaN as compared to a 0.2 eV decrease for our case of epitaxial Au/MoS₂/GaN. However, their absolute values of the GaN BB (1.9–1.6 eV) deviate from our numbers (1.3–1.1 eV) and from the results for bare p -GaN (BB = 0.8 eV)

reported above. The electron affinity of GaN 4.4 eV in the study of Henck *et al* is rather large when compared to other reports in the literature (2.6–4.1 eV) [34–39]. The above discrepancies as well as the spread in the literature of the electron affinities and BB indicate that there is large variation (of several tenths of an eV) of the energy band parameters that depend on the materials state and measurement methods used. The presence of the Au layer in our case, and the different choice of the 2D monolayer (epitaxial versus transferred MoS₂) might also explain the differences with the ARPES results. Regardless, the tendencies and relative changes, as compared to absolute values, in the band values sustain better for different measurement techniques.

The I - V curves at a forward bias above the threshold voltage exhibit some deviation from one measurement (nanodot/domain system) to another (figure 5). We observed a tendency that larger MoS₂ domain triangles, and especially clusters of connected triangles, show larger currents at high biases than smaller domains. This is likely to be the manifestation of the current spreading inside a MoS₂ domain. When the current spreads away from the junction boundary, which is defined by the nanodot, and flows in the in-plane direction inside the MoS₂ domain, an effective increase in the MoS₂/GaN contact area is made accessible by the MoS₂ domain size. The current spreading in the MoS₂/GaN system was shown to exist in our previous study, where we demonstrated via CAFM imaging that larger triangles resulted in more current at the same bias than smaller triangles. Furthermore, it was shown that within one triangle the current diminished in the corners [3]. This present study suggests that the current spreading manifests itself mainly at larger biases and is negligible near the threshold voltages.

While ~99% of the MoS₂ domain triangles are oriented with the GaN lattice, there are occasional monolayer triangles that are misoriented with respect to the substrate lattice. These misoriented triangular domains often exceed by a factor of 2–4 the average size of oriented (epitaxial) MoS₂ triangles. The larger size implies that they grow faster than the epitaxial MoS₂ or nucleate earlier. An example of a MoS₂ triangle that is rotated by 24° with respect to the rest of the epitaxial MoS₂ domains is shown in the SEM image in figure S7. The I - V plot for this triangle is given in figure 5(b), and shows the same threshold voltage $V_{th} = -2.5$ V as for the epitaxial MoS₂, but with higher current levels above V_{th} . The latter could be due to the larger size of misoriented MoS₂ and the current spreading effect described above. Currently, the dearth of misoriented MoS₂ domains precludes a detailed study of such systems.

Another result that comes from the analysis of the I - V curves is that the current at larger biases gradually decreases from measurement-to-measurement on different nanodots. This trend is illustrated in figure 5(c) where the I - V s of several Au nanodots on bare GaN are

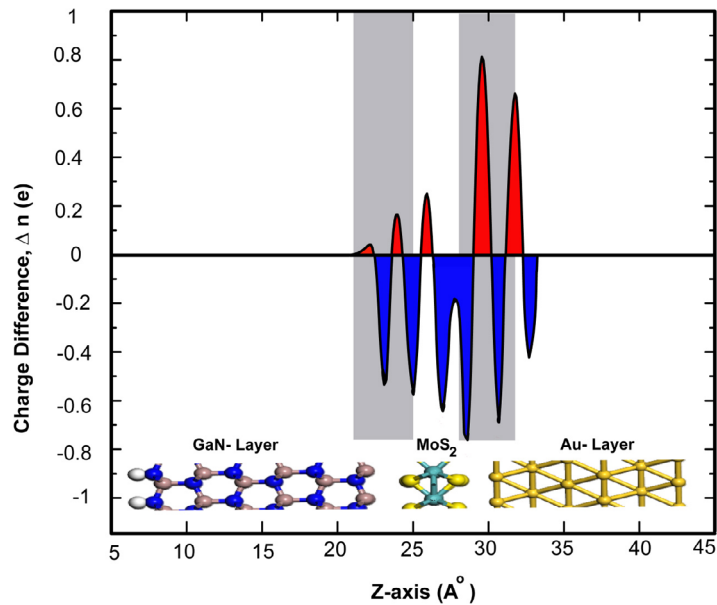


Figure 7. Plane-averaged charge density difference (Δn) of Au (111)/GaN heterostructures before and after MoS₂ layer insertion. Refer to text for the definition of Δn . The spatial location of each layer are marked accordingly. The interface regions are shaded with gray boxes. Blue and red regions indicate the charge depletion and accumulation, respectively. Inset illustrates the atomistic representation of Au, MoS₂ and GaN layers in a Au (111)/MoS₂/GaN heterostructure.

presented. The nanodot numbers in the legend correspond to the sequence of the measurements. During the first few measurements of Au dots 3, 5, and 6 the current magnitude gradually decreases from measurement-to-measurement. At dot 22, the current is substantially smaller above V_{th} (figure 5(c)). This effect is negligible near the threshold voltage $V_{th} = -3.5$ V indicating again that the value of V_{th} and the I - V slope near V_{th} are the intrinsic parameters of the metal-semiconductor junction. Since different independent Au/GaN junctions (# 3, 5, 6, and 22) are measured, the trend must be due to the nanoprobe itself. The degradation (possibly oxidation induced by the current heating) of the W nanoprobe is believed to be the root cause behind this time-dependent observation of the larger contact resistance of the W tip/Au nanodot junction. Additionally, we contacted the GaN substrate with a W nanoprobe (tip) directly, and obtained the I - V of the W/GaN junction (figure 5(c)). Clear rectification was observed for the W/GaN junction corresponding to the p -type SB. The threshold voltage shifted to -4.5 V, and the current level and the slope near V_{th} were substantially reduced. Bare W nanoprobe measurements on MoS₂ triangles were not performed because of possible damage to the monolayers.

Bipolar semiconductor junctions formed with 2D materials are expected to exhibit new physics as compared to conventional pn -junctions. For example, depletion widths are critical parameters of conventional bipolar devices but it is not clear how the depletion regions are formed in a heterojunction with a 2D component that may only be one monolayer thick. Knowing the charge density distribution across the 2D/3D heterojunction can shed light on the origin of the I - V behavior and the Fermi level pinning. The

magnitude of the charge depletion width across the metal/2D and 2D/3D junctions and the Fermi-level pinning (FLP) energy window are the two major effects that define the I - V characteristics in the metal/2D/3D heterostructure. The FLP effect is mainly caused by interface induced dipole formation due to charge redistribution across the metal/2D/3D interface. To address the above issues, we have calculated the plane-averaged charge density difference along the out-of-plane direction in the Au/GaN heterostructure with and without 1L-MoS₂ using the converged charges from our electronic structure calculations. The charge density difference (Δn) along the out-of-plane direction is defined as $\Delta n = n(het) - n(Au_{111}) - n(GaN)$ and is plotted in figure 7. Here, $n(het)$ is the plane averaged charge density of the Au(111)/MoS₂/GaN heterostructure, $n(Au_{111})$ and $n(GaN)$ are the plane averaged charge densities of Au(111) and GaN layers separated by a 10.47 Å vacuum gap (see figure S4). We established in the SD (figure S4) that the interaction between the Au and GaN layers in the absence of the 2D layer is negligible. The charge density distribution in the heterostructure is shown in figure 7 relative to the baseline individual $n(Au_{111})$ and $n(GaN)$ in order to highlight the changes brought about by the 2D monolayer. The degree of charge re-distribution provides an insight into the effect of the MoS₂ monolayer insertion on dipole formation at vdW interfaces.

It is evident from figure 7 that the charge fluctuations around the interfaces are significant in the Au (111)/MoS₂/GaN heterostructure, mainly due to the interactions between GaN and Au (111) layers with the MoS₂ layer. The depletion areas in figure 7 are plotted in blue and have positive net charge due to the withdrawal of electrons. The charge depletion

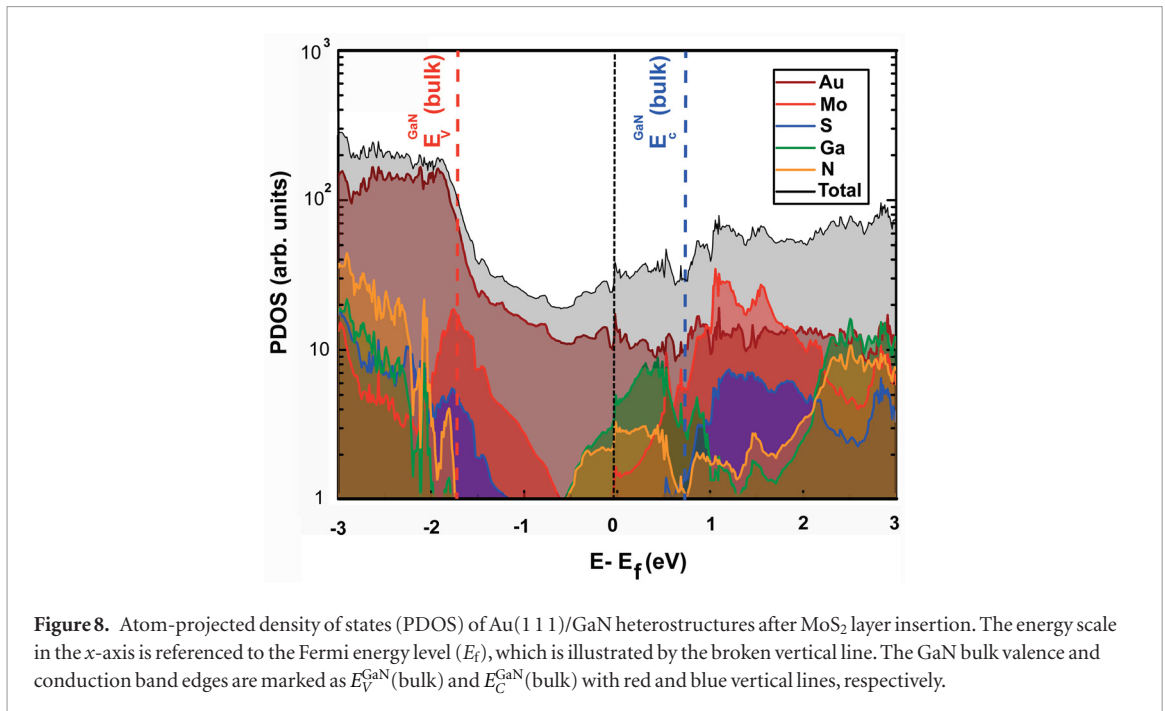


Figure 8. Atom-projected density of states (PDOS) of Au(111)/GaN heterostructures after MoS₂ layer insertion. The energy scale in the x -axis is referenced to the Fermi energy level (E_f), which is illustrated by the broken vertical line. The GaN bulk valence and conduction band edges are marked as $E_v^{\text{GaN}}(\text{bulk})$ and $E_c^{\text{GaN}}(\text{bulk})$ with red and blue vertical lines, respectively.

and accumulation at the GaN/MoS₂ interface is asymmetric compared to the Au (111)/MoS₂. In addition, the depletion width is larger in Au (111)/MoS₂ interface as compared to the GaN/MoS₂ interface, signifying strong interaction through higher degree of states hybridization between the surface Au states and MoS₂ states, mainly d-states from the Mo-atoms. At the GaN/MoS₂ interface, the depletion area of positive charges is higher than the accumulation of the negative charges, indicating larger charge withdrawal by the GaN layer, which results in a larger potential drop across the GaN/MoS₂ interface. However, the depletion width in the GaN layer is minimal because of the weak interaction between GaN and MoS₂ layers which resulted from the larger vdW-gap (4 Å), as compared to 3.3 Å between Au (111) and MoS₂ layers. Due to the strong interaction and states hybridization, the charge from the Au (111) layer extends through the MoS₂ layer into the GaN layer, which is evident by the extension of positive charges throughout the MoS₂ layer. The asymmetric charge accumulation and depletion widths in the GaN/MoS₂ and Au (111)/MoS₂ interfaces are likely one of the causes of the asymmetric threshold voltage V_{th} observed when the polarity of the applied bias is changed.

The charge re-distribution across the interfaces also results in the formation of interface dipoles, which strongly influences the band alignment and SB height. As discussed earlier, the charge fluctuation is conspicuous across the Au (111)/MoS₂/GaN heterojunction, contributing to interface dipole formation, and hence the FLP at the interface. The observed charge fluctuation characteristics are a consequence of the interactions between the energy states of the constituent layers at the heterojunctions. For example, in the Au (111)/MoS₂ heterostructure, the gap states are dominated by hybridized Au and Mo d-states which

results in the FLP, which can be further minimized by surface functionalization of the Au surface [40]. The complexity of the hybridization of the states near the Fermi-level increases significantly in the 3D/2D/metal heterostructure as compared to the cases of the metal/2D and metal/3D heterostructures. In particular, for the GaN/MoS₂/Au (111) heterostructure, MoS₂ states hybridize with both the surface states of GaN and Au. To illustrate this, we plot in figure 8 the atom-projected density of states (PDOS) of Au (111)/GaN heterostructure after the MoS₂ layer insertion. The figure shows in detail how the gap states arise from the overlap of the Mo, S, Ga and Au atomic states, which consequently leads to the FLP. The bulk conduction band and valence band edges of GaN extracted from a separate calculation are marked to illustrate the gap states originating from the MoS₂-GaN and Au-GaN states hybridizations. The observed conduction band offset (CBO) and valence band offset (VBO) between MoS₂ and bulk GaN in the GaN/MoS₂/Au(111) are 0.7 eV and 1.3 eV, respectively. It can be seen that the band offsets (or band alignment) between MoS and GaN deviates from the bulk values when we consider the GaN surface states. Undoped GaN was used in the PDOS calculation that explains the Fermi level position in GaN that differs from the experimental system (compare to figure 6). The observation of the gap states throughout GaN and MoS₂ bandgaps is consistent with the substantial BB due to the FLP observed in the KP measurement, which in turn reduces the effect of the SB and complicates the device design. The functionalization or surface passivation of both the Au and GaN surfaces might be one of the possible solutions to minimize the FLP and improve the control on the SB.

This work is a part of an effort to explore possible advantages to high-speed and high-power microwave devices from the concept of the integration of 2D

semiconductor crystals with III–Vs in vertical heterostructures.

4. Conclusion

The integration of a monolayer 2D semiconductor with conventional (3D) semiconductors and metals was explored in order to build the scientific framework needed to develop hybrid 2D/3D heterostructure electronic devices. All-epitaxial Au/1L-MoS₂/GaN heterostructures were fabricated with MOCVD, powder vaporization, and e-beam evaporation and compared to Au/GaN junctions. Nanostructures consisting of Au/GaN with and without 1L-MoS₂ present at the interface were evaluated with cross-sectional TEM. The atomic plane spacing between Mo and Ga planes (2D–3D distance) and Au to Mo planes were measured to be $6.1 \pm 0.3 \text{ \AA}$ and $4.5 \pm 0.4 \text{ \AA}$, respectively, which are consistent with first principle calculated values.

Current–voltage characteristics of the vertical heterojunctions were measured and show that the charge transport was dominated by the Au/GaN interface with the vdW 2D material acting as a perturbation. The site-resolved charge density and potential profiles calculated using the first principles method elucidated the role of the 2D layer in the formation of the potential barrier and showed the depletion regions within the mixed-dimensional bipolar junction. The Schottky barrier heights (SBH) extracted from I – V s are 1.3 eV for the Au/MoS₂/ p -GaN heterostructure and 1.5 eV for the Au/ p -GaN heterostructure, indicating a reduction in the barrier height by 0.2 eV when MoS₂ is present. The SBH values suggest Fermi level pinning and substantial BB in GaN at the interface. The formation of gap states leading to Fermi level pinning was supported by our first principles calculations of the atom-projected density of states in the heterojunction. This study provides quantitative information and insight on the nanostructural and electrical aspects of the interactions of a semiconductor 2D monolayer with III–V semiconductors, a mainstay of modern high speed electronics, and metals.

Acknowledgments

This work was supported by the US Army Research Laboratory (ARL) Director's Strategic Initiative (DSI) program on understanding the transport in complex crystalline materials based on vdW heterostructures. This work was supported by grants of computer time from the DOD High Performance Computing Modernization Program at the US Air Force Research Laboratory and US Army Engineer Research and Development Center DoD Supercomputing Resource Centers. DR and AVD acknowledge the support of Material Genome Initiative funding allocated to NIST. JAR acknowledges support of the National Science

Foundation under grant number DMR-1453924. DR is grateful to Dr. Igor Levin (NIST) for the help with the CBED analysis.

Author contributions

The manuscript was written through contributions of all authors. All authors have given approval to the final version of the manuscript.

Supplementary data

The following file is available free of charge. Proof of the epitaxy of MoS₂ on GaN and Au on GaN, details on the first principles simulations of 2D/3D heterostructures, TEM measurements of the nanodot/substrate contact angles, SB evaluation from the I – V s (MoS₂_nanodots - submission2018-04-30—SD.pdf).

ORCID iDs

Dmitry Ruzmetov  <https://orcid.org/0000-0002-0688-1908>

Robert A Burke  <https://orcid.org/0000-0002-1772-9848>

References

- [1] Manzeli S, Ovchinnikov D, Pasquier D, Yazyev O V and Kis A 2017 2D transition metal dichalcogenides *Nat. Rev. Mater.* **2** 17033
- [2] Schwierz F, Pezoldt J and Granzner R 2015 Two-dimensional materials and their prospects in transistor electronics *Nanoscale* **7** 8261–83
- [3] Ruzmetov D *et al* 2016 Vertical 2D/3D semiconductor heterostructures based on epitaxial molybdenum disulfide and gallium nitride *ACS Nano* **10** 3580–8
- [4] Torres C M *et al* 2015 High-current gain two-dimensional MoS₂-base hot-electron transistors *Nano Lett.* **15** 7905–12
- [5] Song I, Park C and Choi H C 2015 Synthesis and properties of molybdenum disulfide: from bulk to atomic layers *RSC Adv.* **5** 7495–514
- [6] Rigosi A F, Hill H M, Rim K T, Flynn G W and Heinz T F 2016 Electronic band gaps and exciton binding energies in monolayer Mo_xW_{1-x}S₂ transition metal dichalcogenide alloys probed by scanning tunneling and optical spectroscopy *Phys. Rev. B* **94** 075440
- [7] Sze S M 1990 *High Speed Semiconductor Devices* (New York: Wiley)
- [8] Jariwala D, Marks T J and Hersam M C 2017 Mixed-dimensional van der Waals heterostructures *Nat. Mater.* **16** 170–81
- [9] Fletcher A S A and Nirmal D 2017 A survey of gallium nitride HEMT for RF and high power applications *Superlattices Microstruct.* **109** 519–37
- [10] O'Regan T P *et al* 2017 Structural and electrical analysis of epitaxial 2D/3D vertical heterojunctions of monolayer MoS₂ on GaN *Appl. Phys. Lett.* **111** 051602
- [11] Lee E W, Lee C H, Paul P K, Ma L, McCulloch W D, Krishnamoorthy S, Wu Y Y, Arehart A R and Rajan S 2015 Layer-transferred MoS₂/GaN PN diodes *Appl. Phys. Lett.* **107** 103505
- [12] Gupta P *et al* 2016 Layered transition metal dichalcogenides: promising near-lattice-matched substrates for GaN growth *Sci. Rep.* **6** 23708
- [13] Tangi M *et al* 2016 Determination of band offsets at GaN/single-layer MoS₂ heterojunction *Appl. Phys. Lett.* **109** 032104

- [14] Krishnamoorthy S, Lee E W, Lee C H, Zhang Y W, McCulloch W D, Johnson J M, Hwang J, Wu Y Y and Rajan S 2016 High current density 2D/3D MoS₂/GaN Esaki tunnel diodes *Appl. Phys. Lett.* **109** 183505
- [15] Henck H et al 2017 Interface dipole and band bending in the hybrid p-n heterojunction MoS₂/GaN(0001) *Phys. Rev. B* **96** 115312
- [16] Wan Y et al 2018 Epitaxial single-layer MoS₂ on GaN with enhanced valley helicity *Adv. Mater.* **30** 1703888
- [17] Sze S M 1981 *Physics of Semiconductor Devices* (New York: Wiley)
- [18] Zhang K H et al 2018 Large scale 2D/3D hybrids based on gallium nitride and transition metal dichalcogenides *Nanoscale* **10** 336–41
- [19] Kim C, Moon I, Lee D, Choi M S, Ahmed F, Nam S, Cho Y, Shin H J, Park S and Yoo W J 2017 Fermi level pinning at electrical metal contacts of monolayer molybdenum dichalcogenides *ACS Nano* **11** 1588–96
- [20] Kang J H, Liu W, Sarkar D, Jena D and Banerjee K 2014 Computational study of metal contacts to monolayer transition-metal dichalcogenide semiconductors *Phys. Rev. X* **4** 031005
- [21] Gong C et al 2013 Metal contacts on physical vapor deposited monolayer MoS *ACS Nano* **7** 11350–7
- [22] Burke R A et al 2018 Epitaxial growth of molybdenum disulfide on gallium nitride submitted
- [23] Saxler A, Kung P, Zhang X, Walker D, Solomon J, Ahoujja M, Mitchel W C, Vydyanath H R and Razeghi M 1997 GaN doped with sulfur *Defects in Semiconductors—Icids-19, Pts 1–3* vol **258–63**, ed G Davies and M H Nazare (Zurich-Uetikon: Transtec Publications Ltd) pp 1161–6
- [24] Blochl P E 1994 Projector augmented-wave method *Phys. Rev. B* **50** 17953–79
- [25] Kresse G and Furthmuller J 1996 Efficient iterative schemes for *ab initio* total-energy calculations using a plane-wave basis set *Phys. Rev. B* **54** 11169–86
- [26] Petkov V, Billinge S J L, Larson P, Mahanti S D, Vogt T, Rangan K K and Kanatzidis M G 2002 Structure of nanocrystalline materials using atomic pair distribution function analysis: study of LiMoS₂ *Phys. Rev. B* **65** 092105
- [27] Rhoderick E H and Williams R H 1988 *Metal-Semiconductor Contacts* (Oxford: Clarendon)
- [28] Iucolano F, Roccaforte F, Giannazzo F and Raineri V 2007 Temperature behavior of inhomogeneous Pt/GaN Schottky contacts *Appl. Phys. Lett.* **90** 092119
- [29] Im J S, Moritz A, Steuber F, Harle V, Scholz F and Hangleiter A 1997 Radiative carrier lifetime, momentum matrix element, and hole effective mass in GaN *Appl. Phys. Lett.* **70** 631–3
- [30] Ke W C, Lee S J, Chen S L, Kao C Y and Houng W C 2012 Effects of growth conditions on the acceptor activation of Mg-doped p-GaN *Mater. Chem. Phys.* **133** 1029–33
- [31] Ahmed F, Choi M S, Liu X and Yoo W J 2015 Carrier transport at the metal-MoS₂ interface *Nanoscale* **7** 9222–8
- [32] Card H C and Rhoderick E H 1971 Studies of tunnel MOS diodes 1. Interface effects in silicon schottky diodes *J. Phys. D: Appl. Phys.* **4** 1589
- [33] Yu L S, Qiao D, Jia L, Lau S S, Qi Y and Lau K M 2001 Study of Schottky barrier of Ni on p-GaN *Appl. Phys. Lett.* **79** 4536–8
- [34] Pearson S J, Abernathy C R and Ren F 2006 *Gallium Nitride Processing for Electronics, Sensors and Spintronics* (Berlin: Springer)
- [35] Tracy K M, Mecouch W J, Davis R F and Nemanich R J 2003 Preparation and characterization of atomically clean, stoichiometric surfaces of n- and p-type GaN(0001) *J. Appl. Phys.* **94** 3163–72
- [36] Lin S C, Kuo C T, Liu X G, Liang L Y, Cheng C H, Lin C H, Tang S J, Chang L Y, Chen C H and Gwo S 2012 Experimental determination of electron affinities for InN and GaN polar surfaces *Appl. Phys. Express* **5** 031003
- [37] Bougrov V, Levinshtein M, Rumyantsev S and Zubrilov A 2001 Gallium nitride (GaN) *Properties of Advanced Semiconductor Materials: GaN, AlN, InN, BN, SiC, SiGe* ed M S Levinshtein et al (New York: Wiley)
- [38] Korotkov R Y, Gregie J M and Wessels B W 2002 Optical properties of the deep Mn acceptor in GaN: Mn *Appl. Phys. Lett.* **80** 1731–3
- [39] Wu C I, Kahn A, Taskar N, Dorman D and Gallagher D 1998 GaN (0001) – (1 × 1) surfaces: Composition and electronic properties *J. Appl. Phys.* **83** 4249–52
- [40] Min K A, Park J, Wallace R M, Cho K and Hong S 2014 Reduction of Fermi level pinning at Au–MoS₂ interfaces by atomic passivation on Au surface *2D Mater.* **4** 015019